Heliyon 9 (2023) e16942

Contents lists available at ScienceDirect

Heliyon

journal homepage: www.cell.com/heliyon

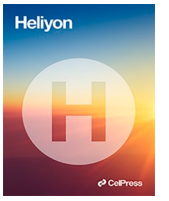

Detection of delamination of steel–polymer sandwich composites using acoustic emission and development of a forming limit diagram considering delamination

Jewook Yang [1], Sungjin Han [1], Woong-Ryeol Yu [*]

Department of Materials Science and Engineering and Research Institute of Advanced Materials, Seoul National University, 1 Gwanak-ro, Gwanak-gu, Seoul, 151-744, Republic of Korea

ARTICLE INFO

Keywords:
Acoustic emission
Delamination
Finite element analysis
Forming limit diagram
Steel–polymer sandwich composites

ABSTRACT

The formability of steel–polymer sandwich composites was investigated using a new forming limit diagram (FLD) while considering delamination and fracture. The acoustic emission (AE) technique was used to observe delamination during the forming process. Several tests, including tensile and lap shear tests, were performed to identify the AE features of delamination. In addition, finite element simulations were carried out using the cohesive zone model to predict the delamination of steel–polymer sandwich composites. An FLD of the sandwich composite was also constructed using the finite element model. Finally, the effect of interfacial adhesion on the formability of sandwich composites was investigated, from which the optimal condition for interfacial adhesion (in terms of ensuring the formability of the sandwich composite) was obtained.

1. Introduction

Steel–polymer sandwich composites have advantages such as improved specific weight and enhanced energy absorption characteristics while having comparable bending stiffness with the monolithic steel sheet [1]. In addition, due to the core polymer, steel–polymer sandwich composites exhibit multifunctional properties, such as acoustic damping and heat insulation [2]. Due to their favorable properties, laminated steel–polymer sandwich sheets have been widely used to replace monolithic steel sheets in automotive, aerospace and construction industries [3].

Various forming methods have been used to produce metal–polymer sandwich composites such as deep drawing [4], injection forming [5] and roll bonding [6]. Furthermore, incremental forming was recently developed to extend forming potential of the sandwich laminates [7]. Despite these manufacturing techniques, various failure mechanisms such as delamination, skin sheet cracking, and core polymer failure are major obstacles that make it difficult to accurately determine the formability of sandwich composite parts. Delamination, in particular, occurs during forming process due to the different lengths of the metal skin layers, resulting in high shear forces in the interfaces [8]. Therefore, it is essential to characterize the formability of sandwich composites considering delamination to evaluate forming methods effectively.

Extensive researches have been conducted on characterizing forming limit of metal–polymer sandwich composites. One of the most

* Corresponding author.
E-mail address: woongryu@snu.ac.kr (W.-R. Yu).
[1] These authors contributed equally to this work.

https://doi.org/10.1016/j.heliyon.2023.e16942
Received 25 May 2023; Received in revised form 31 May 2023; Accepted 1 June 2023
Available online 2 June 2023

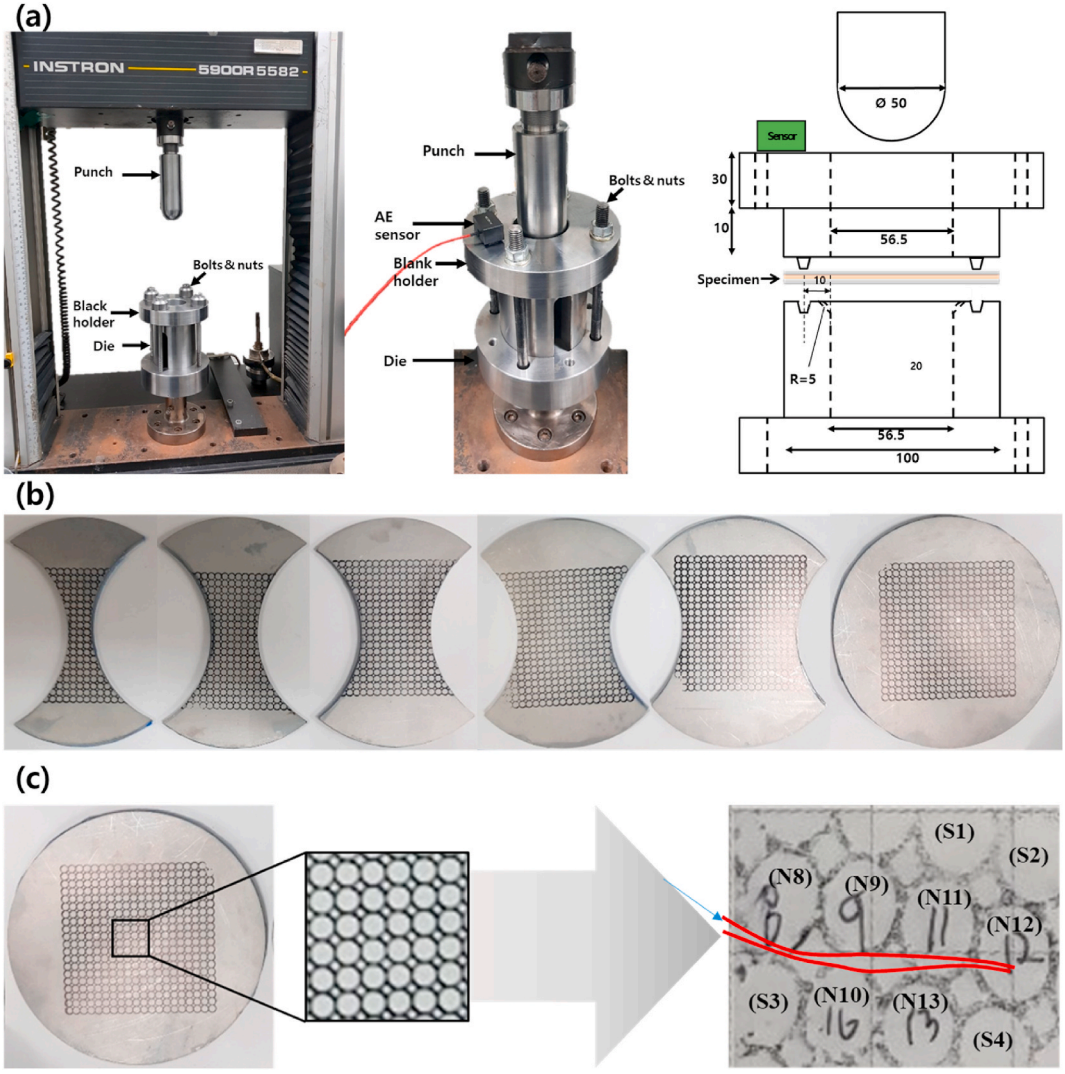

Fig. 1. (a) Punch test set-up, (b) specimen geometry for the Nakazima punch test, and (c) circular grids printed on the specimen with a stamp (left) and grids of the deformed specimen (right).

widely used to characterize formability of sheet material is forming limit diagram (FLD) [9]. Several studies have investigated the effect of change in constituent of sandwich composites. Typically, the FLD is built by analyzing the failure of bottom metal sheet [10, 11]. Furthermore, studies have shown that increasing the core thickness improves the formability [12,13], and that the mechanical properties of the core polymer can also improve the formability of metal–polymer sandwich composites [14,15].

There have been some researches to investigate the delamination of metal-polymer sandwich composites. Kazemi et al. performed forming test of steel–polyethylene sandwich composites and observed noticeable delamination based on the SEM investigation [16]. However, since the SEM image was observed after all fractures had occurred, the forming limit at the moment of delamination could not be observed. While they provided information on whether delamination occurred or not, they did not indicate *the moment* exactly the delamination occurred. Son et al. constructed an FLD for a multilayer sheet material (steel–polyvinyl chloride–polyethylene terephthalate) based on delamination [17]. They used a CCD camera during the forming process to optically observe *the moment* of delamination between the steel and polymer–coated layers, but only the delamination to the surface was observed. To construct a FLD of sandwich composites based on delamination, a technique to not only detect delamination on the surface but also capture the moment of delamination in areas that are not optically observable is required.

This study proposes a new process for constructing the FLD of a steel–polymer sandwich composites based on delamination. Our new process provides information on the moment of delamination in areas that are not optically observable, providing comprehensive delamination information across the entire component. For our purpose, the acoustic emission (AE) technique was used during the formability testing. Several tests were carried out to identify the characteristic AE features associated with the failure modes of the sandwich composites. Then, a punch test was performed with AE monitoring. Using the AE signals of delamination, a new FLD of the

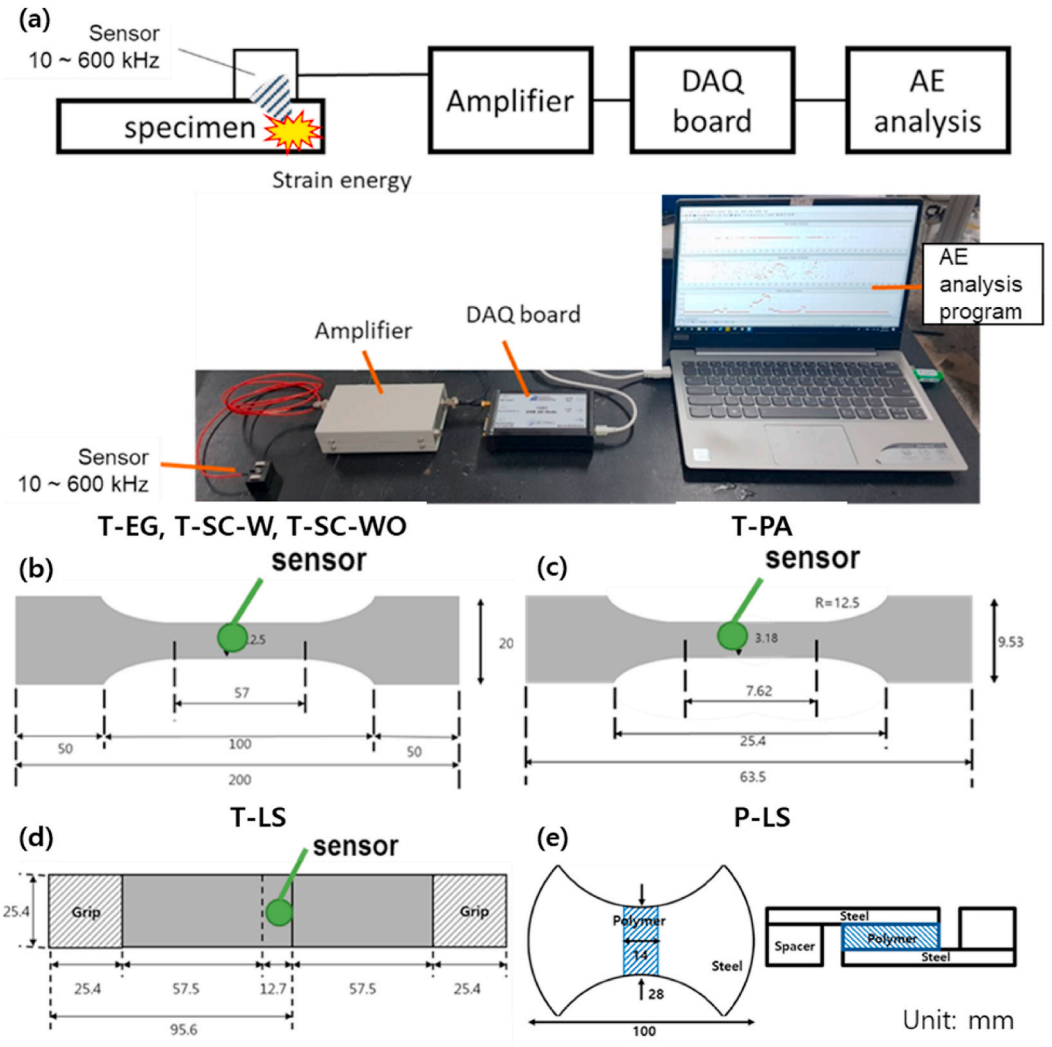

Fig. 2. (a) Acoustic emission (AE) test set-up, (b) steel and composite tensile specimens (T-EG, T–SC–W, T–SC–WO), (c) polymer tensile test specimen (T-PA), (d) lap shear test specimen (T-LS), and (e) punch shear test specimen (P-LS) used to observe AE features.

steel–polymer sandwich composites was constructed. Additionally, the formability tests were simulated using the cohesive zone model to consider interfacial properties, and the effect of interfacial adhesion on the formability of the sandwich composite was investigated.

2. Experimental

2.1. Sandwich composites preparation

An electrogalvanized (EG) steel sheet with a thickness of 0.6 mm (POSCO, Korea) was used as the skin material for the sandwich composite. A polyamide-6 (PA) sheet with a thickness of 1 mm (Goodfellow, UK) was used as the core material. The total thickness of the EG steel–PA–EG steel (EG–PA–EG) sandwich composite was 2.2 mm. A cyanoacrylate adhesive, Loctite 401, was used to bond the skin and core sheets together. After adhesive applied, sandwich sheet was heated at 120 °C with 0.0015 MPa pressure for 3 h.

2.2. Punch test

Nakazima test [18] using hemispherical punch was selected as the forming process of steel–polymer composites in this study. Fig. 1 (a) shows the punch test set-up based on a 100-kN universal testing machine (Instron 5582; Instron, Norwood, MA, USA). The diameter of the hemispherical punch was 50 mm and that of the die cavity was 56.5 mm.

A specimen was placed on the die and then clamped by the blank holder using nuts and bolts. The beads on the blank holder ensured that the specimen did not slip. The punch descended at a crosshead speed of 10 mm/min. Sandwich composite specimens prepared for

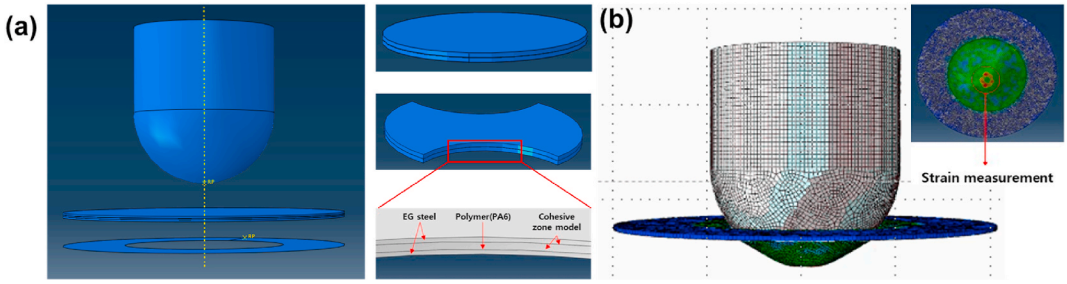

Fig. 3. Simulation models for the (a) punch test and steel–polymer sandwich composite. (b) An example of punch test simulation result. (color should be used). (For interpretation of the references to color in this figure legend, the reader is referred to the Web version of this article.)

the Nakajima forming test are shown in Fig. 1(b) [19]. Circular specimens 100 mm in diameter, and hourglass-shaped specimens with neck widths of 10, 20, 30, 40, and 50 mm, were used. Due to their geometrical shape, each specimen was designed to have different strain paths from uniaxial to biaxial tension.

Circular (3-mm-diameter) grids were printed on specimens using a stamp (Fig. 1(c) left). The grid on deformed ("failed") specimens was transferred to a flat surface using tape. The major and minor strains were identified by measuring the deformed grids on the tape. Safe and neck/fracture regions were determined [20]. The nearest unnecked grids were considered as safe regions, while necked and fractured grids were classified as neck/fracture regions (see Fig. 1(c) right). Then, the forming limit curve was plotted above the strains of the safe region and below the strains of the neck/fracture region.

2.3. Observing delamination using acoustic emission

2.3.1. Equipment

An AE system was used to establish the moment of delamination during the punch test (Fig. 2(a)). First, a broadband-type transducer (M204A; Fuji Ceramics Corporation, Japan) collected wave signals. The transducer had a diameter of 5.5 mm and operated at 10–600 kHz. Then, a Fuji Ceramics Corporation amplifier amplified the AE signal. A single-channel data acquisition board (Mistras 1283 USB AE Node; Physical Acoustic Corporation, USA) was used to record the AE data. Acoustic emission software (WIN; Mistras, USA) was used to analyze the wave signals. To ensure good acoustic coupling, silicone grease was applied to the surface of the transducer, which was fixed to a magnetic support. The intensity of wave acquisition was calibrated using a pencil-break test.

2.3.2. Test procedures

We conducted two types of tests to obtain acoustic emission (AE) signal features. The first type of test involved performing tensile tests on monolithic layers of steel (T-EG) and polymer (T-PA) according to ASTM E8 [21] and D638 [22] standards, respectively. The geometry of the steel and polymer specimens used in these tests are shown in Fig. 2(b) and (c), respectively. Punching tests of monolithic EG steel (P-EG) were also conducted to confirm that the AE signal features are generated in the punching test environment. The sensor was attached to the blank holder as shown in Fig. 1(a).

For the second type of test, delamination of sandwich composites was induced using the lap shear test (T-LS) according to the ASTM D3164 [23] standard, and the geometry of the lap shear specimen is shown in Fig. 2(d). Tensile testing of the steel–polymer sandwich composites with (T–SC–W) and without (T–SC–WO) adhesion was also conducted with the specimen geometry shown in Fig. 2(b). Next, the punch shear test specimen (P-LS) was designed such that delamination was the primary failure mode (Fig. 2(e)). When the hemispherical punch pushed the middle region of the specimen, shear force was generated between the steel and polymer layers, and delamination finally occurred. The sensor was attached to the blank holder as shown in Fig. 1(a).

3. Numerical simulation

Numerical FLD of steel–polymer composite was constructed to compare with experimental results and confirm the theoretical validity of experimental FLD. Additionally, we used the numerical FLD to investigate the influence of interfacial properties on the formability of the sandwich composites. In Section 3.1, built-in models used to simulate the punch test are introduced, followed by the material parameter identification for these models in Section 3.2.

3.1. Numerical model

To simulate the punch test, finite element analysis software (ABAQUS/Standard; Simulia Inc., USA) was used. Following the actual experiments, three-dimensional solid models were generated; the geometries of the model and specimen are provided in Fig. 3(a). An example of punch test simulation result and strain measurement region is shown in Fig. 3(b). Delamination between the steel skin and core polymer was considered in the cohesive element layer. The thickness of this layer was set to be 0.01 mm. Tie constraints were used to connect the cohesive elements to the steel and polymer elements.

Isotropic elastic, J2 plastic, ductile fracture criterion, and damage evolution built-in models were used to simulate steel and

Table 1
Material parameters of EG steel used for the simulations.

Elastic-plastic behavior (EG steel)			
Elastic modulus	**Poisson's ratio**	**Yield strength**	**Tensile strength**
190.4 GPa	0.3	131.2 MPa	250.3 MPa
Ductile damage (EG steel)			
Failure strain	**Stress triaxiality**		**Strain rate**
0.29	0.33		0.0083 s-1
Damage evolution (EG steel)			
Fracture toughness		10 N/mm	
Elastic-plastic behavior (PA)			
Elastic modulus	**Poisson's ratio**	**Yield strength**	**Tensile strength**
2905 MPa	0.33	32.2 MPa	53.0 MPa

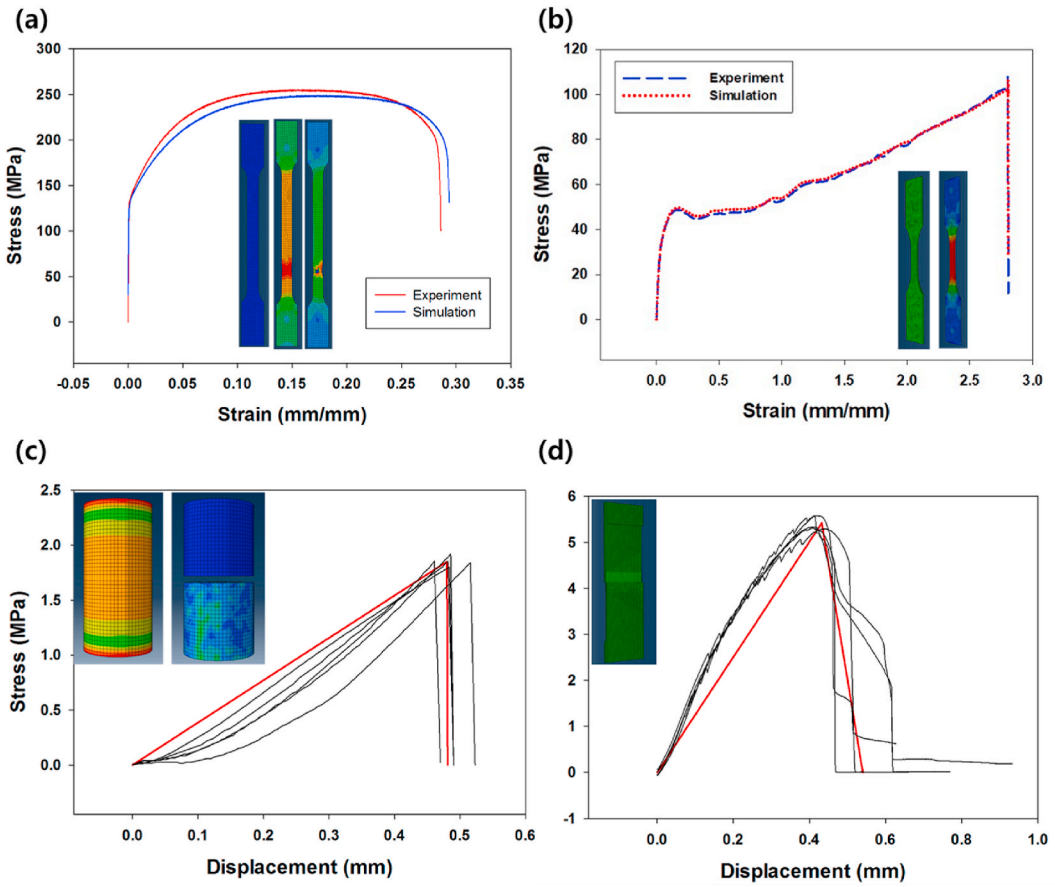

Fig. 4. Comparison of experimental and re-simulation results for the tensile behavior of (a) steel and (b) polymer, and the results of (c) butt joint and (d) lap shear tests.

polymer behaviors. J2 plasticity model is adequate for simulating the properties of the core polymer in the punch test since the effect of temperature and strain rate are negligible. The ductile failure criterion, a phenomenological model, was used to predict the onset of material damage as suggested by Ref. [24]. Equivalent plastic strain ($\bar{\varepsilon}_D^{pl}$) was determined as a function of stress triaxiality (η) using Equation (1) [24]. Stress triaxiality is $\eta = \sigma_m/\sigma_{eq}$, where σ_m is mean stress and σ_{eq} is Von Mises equivalent stress. When Equation (1) was satisfied, softening of the yield stress and degradation of elasticity occurred [25].

Table 2
Material parameters required by the cohesive zone model.

	Mode I	Mode II	Mode III
Failure strength (MPa)	1.85	5.36	
Fracture toughness (N/mm)	0.36	0.8	
Stiffness (N/mm^3)	10^6		
Mesh size (mm)	0.01		

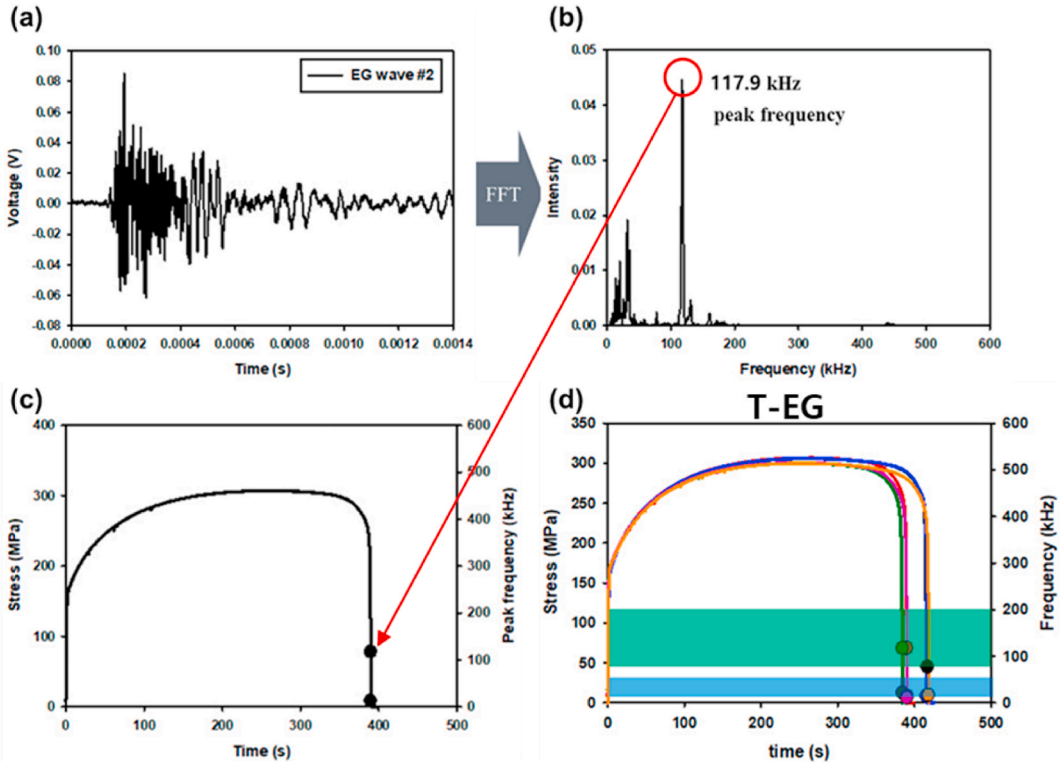

Fig. 5. (a) AE waveform recorded, (b) fast Fourier transform result of the waveform, (c) peak frequency distribution plot, and (d) peak frequency band plot of T-EG.

$$\int \frac{d\bar{\varepsilon}^{pl}}{\bar{\varepsilon}_D^{pl}(\eta)} = 1 \tag{1}$$

Previous researches have simulated the delamination in metal–polymer sandwich composites using cohesive zone model [26,27]. This model involves the use of cohesive elements that determine delamination according to the traction–separation law [28]. Among various types of traction–separation laws, a bilinear law was selected due to its efficiency with respect to CPU time. The bilinear law consists of two stages. In the pre-delamination stage, the cohesive element follows elastic traction-separation relations given by Equation (2).

$$\begin{pmatrix} \sigma_n \\ \sigma_t \\ \sigma_l \end{pmatrix} = \begin{pmatrix} K_n & 0 & 0 \\ 0 & K_t & 0 \\ 0 & 0 & K_l \end{pmatrix} \begin{pmatrix} \delta_n \\ \delta_t \\ \delta_l \end{pmatrix} \tag{2}$$

where σ and δ represent traction and separation, respectively, and n, t and l denote the normal, tangential and longitudinal directions. K denotes the interfacial stiffness. When the traction in cohesive element reaches the maximum traction, delamination is initiated, and the post-delamination stage begins. Delamination propagates until the energy release rate reaches the critical fracture energy. The energy release rates (G_i) and critical fracture energy ($G_{i,c}$) are expressed as Equations (3) and (4), respectively.

$$G_i = \int \sigma_i d\delta_i, i = n, t, l \tag{3}$$

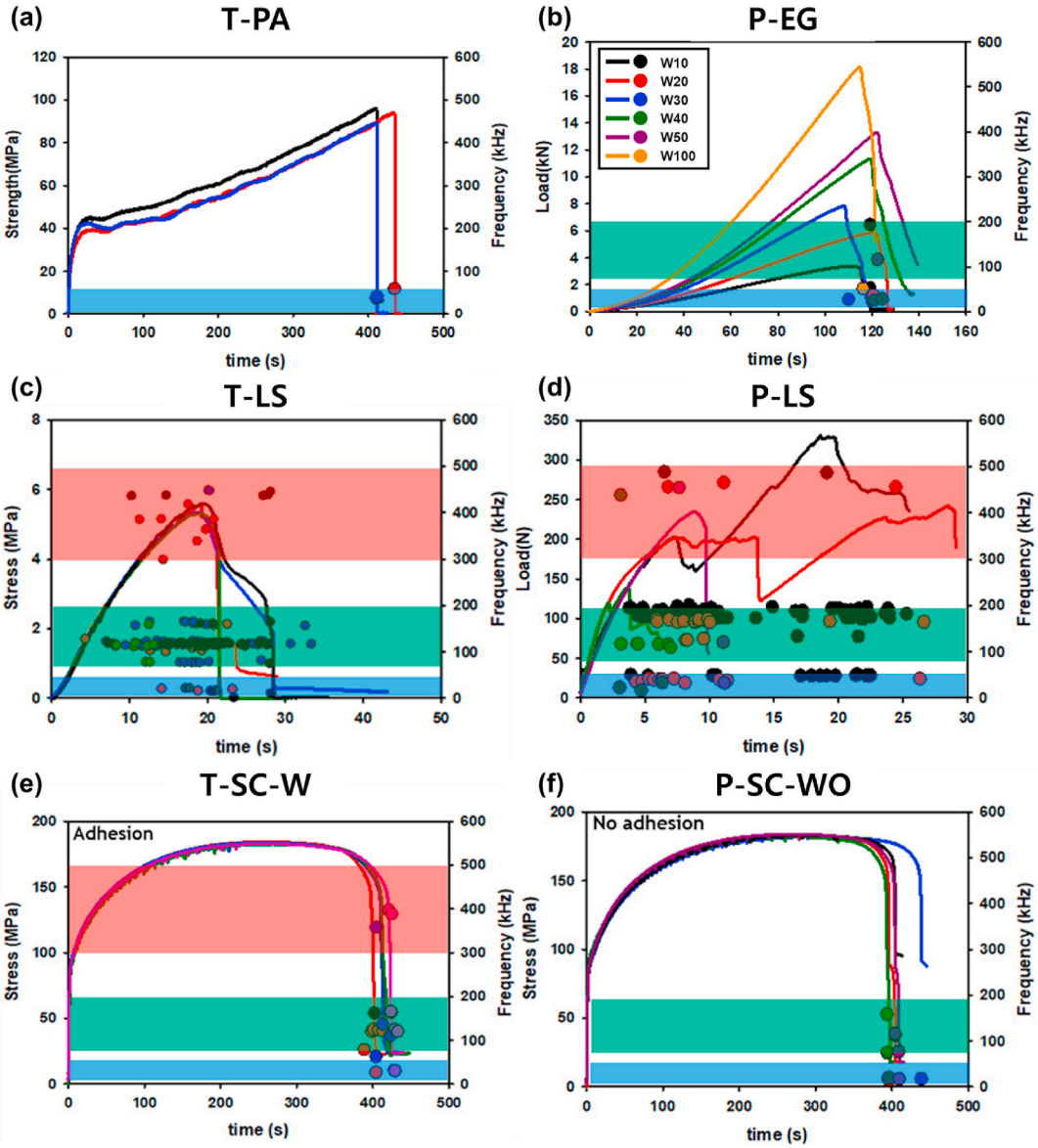

Fig. 6. Peak frequency band plots of (a) polymer tensile test (T-PA), (b) steel punch test (P-EG), (c) lap shear (T-LS) and (d) punch shear tests (P-LS). Peak frequency band plots of a steel–polymer composite tensile test. Specimens (e) with adhesive (T–CS–W) and (f) without adhesive (T–CS–WO).

$$G_{i,c} = \int \sigma_{i,c} d\delta_{i,c}, i = n, t, l \tag{4}$$

where $\sigma_{i,c}$ is failure strength, and $\delta_{i,c}$ is critical separation length of cohesive zone model. The quadratic criterion (Equation (5)) suggested by Ye [29] was used to evaluate the failure initiation value that induces delamination. The power law criterion (Equation (6)) suggested by Long [30] was used to evaluate failure propagation criterion for continued delamination.

$$\sum \left(\frac{\sigma_i}{\sigma_{i,c}}\right)^2 = 1, i = n, t, l \tag{5}$$

$$\sum \left(\frac{G_i}{G_{i,c}}\right) = 1, i = n, t, l \tag{6}$$

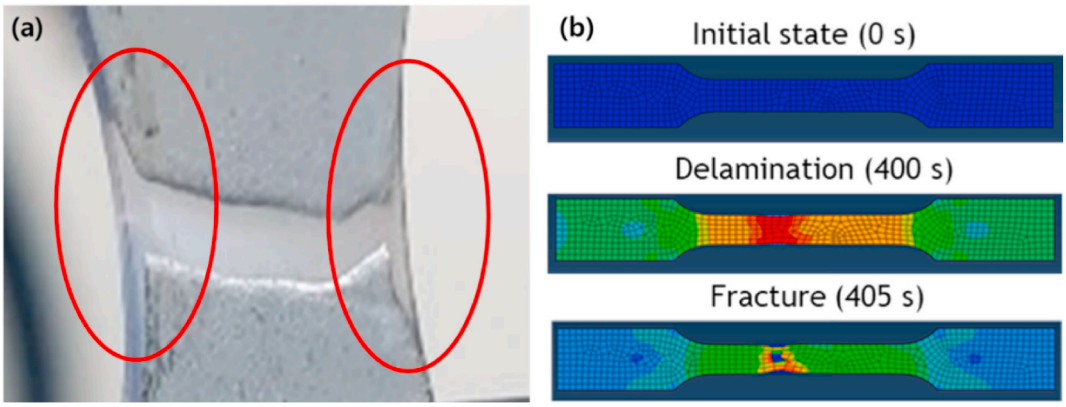

Fig. 7. (a) Observed delamination area after tensile testing of the steel–polymer sandwich composite (T–SC–W) and (b) results of numerical simulation. (color should be used). (For interpretation of the references to color in this figure legend, the reader is referred to the Web version of this article.)

Fig. 8. Peak frequency bands of each failure mode for the steel–polymer sandwich composite. (color should be used). (For interpretation of the references to color in this figure legend, the reader is referred to the Web version of this article.)

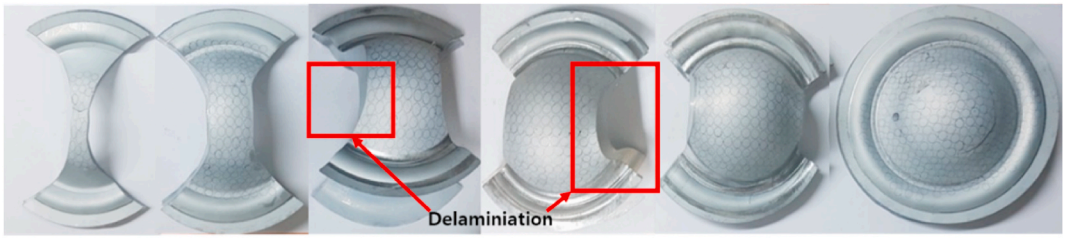

Fig. 9. Deformed specimens after the punch test. (color should be used). (For interpretation of the references to color in this figure legend, the reader is referred to the Web version of this article.)

3.2. Material parameter identification

Uniaxial tensile tests were conducted on monolithic steel and PA sheets, and the resulting material parameters are presented in Table 1. Fracture toughness was set to be 10 N/mm. Using these material parameters and the models described earlier, tensile tests were re-simulated, and the results have a good agreement with the measurements, as shown in Fig. 4(a) and (b).

To determine four interfacial properties ($\delta n,c$, $\delta t,c = \delta l,c$, Gn,c, $Gt,c = Gl,c$) required for the bilinear law, four different experiments were carried out including butt joint, lap shear, double cantilever beam, and end-notched flexure tests [31]. The interfacial stiffness for the cohesive element was set to be 10^6 N/mm^3 following the previous studies [32–34]. All material constant values for the cohesive zone model are provided in Table 2. The butt joint and lap shear tests were then re-simulated, and results were in good agreement with the measurements, as shown in Fig. 4(c) and (d).

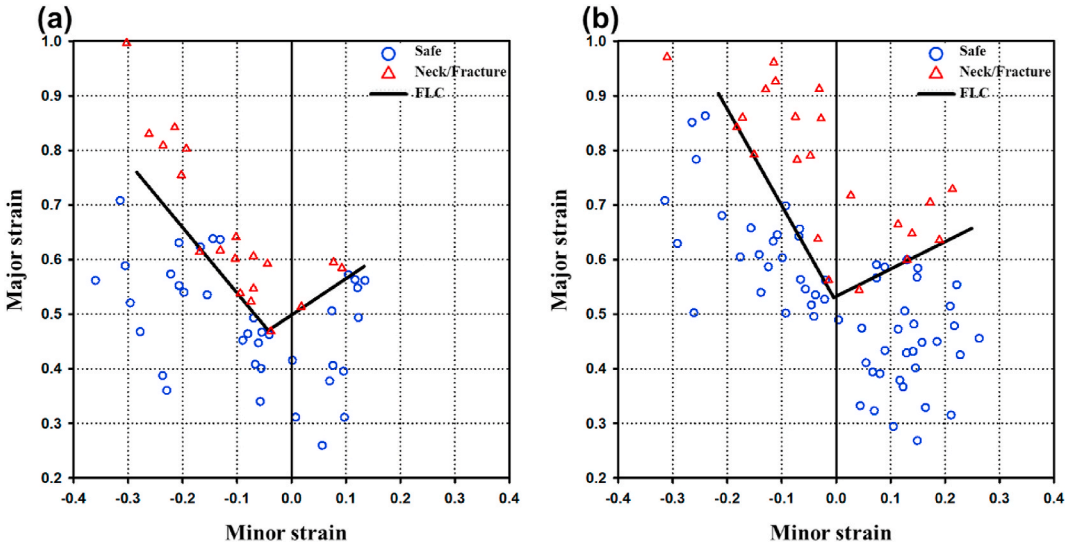

Fig. 10. Experimental forming limit diagram (FLD). (a) Electrogalvanized (EG) monolayer steel sheet and (b) EG steel–polyamide-6–EG steel (EG–PA–EG) sandwich composite.

4. Result and discussion

4.1. AE signal features

Previous studies have utilized five AE parameters (amplitude, duration, energy, rise time, and peak frequency) to classify the failure modes of composite materials. Among these parameters, peak frequency has been identified as the most significant by researchers [35–37]. Therefore, in this study, we transformed AE signals to frequency domain using fast Fourier transform (FFT) to extract peak frequency information. The method for identifying delamination AE signal features using peak frequency will be described below.

An example of AE signals obtained from T-EG is shown in Fig. 5(a), and its FFT result is shown in Fig. 5(b). First, the time at which the AE signals was generated was plotted on the x-axis, and the peak frequency of the AE signals was plotted on the y-axis to create a peak frequency plot. Next, the peak frequency plot was overlaid with the load-time plot to generate a peak frequency distribution plot. Fig. 5(c) shows the peak frequency distribution plot of the T-EG as an example. The peak frequency distribution plot of each test is analyzed, and the "frequency bands" are defined by clustering the peak frequency that appears repeatedly, to be used for classification of failure mechanisms. For each test, frequency bands are visually defined: frequency between 10 and 50 kHz (blue band); frequency between 70 and 200 kHz (green band); and frequency between 300 and 500 kHz (red band). For an example frequency bands of T-EG are shown in Fig. 5(d).

The peak frequency band plot for the tests conducted in Section 2.3.2 are presented in Figs. 5(d) and Fig. 6. The blue and green frequency bands are visible in all the tests. In the case of T-EG, T-PA, P-EG, T–SC–W, and T–SC–WO, these bands begin at the onset of both steel and polymer fractures, as shown in Figs. 5(d), Fig. 6(a), (b), (e) and (f). Thus, these frequency bands can be considered as characteristic features of steel and polymer fractures.

The red frequency band was observed in the T-LS (Fig. 6(c)) and P-LS (Fig. 6(d)) tests, and it was continuously generated throughout these tests. Therefore, the red frequency band is considered an indicator of delamination.

When comparing T–SC–W and T–SC–WO, it was found that the steel–polymer composite specimens containing adhesive between layers displayed an additional red frequency band at the same time as steel fracture, which was not observed in the specimens without adhesive. In T–SC–W, it was observed from the specimen broken that delamination had occurred, as shown in Fig. 7(a). Furthermore, numerical simulation of T–SC–W showed that delamination was observed slightly before the steel skin was broken, as shown in Fig. 7 (b). The time at which delamination occurred coincided with the time at which the AE signals appeared in Fig. 6(e).

The peak frequency bands of each failure mode in the steel–polymer sandwich composites are listed in Fig. 8; these were then used to detect delamination during formability testing and construction of an FLD considering delamination.

4.2. Forming limit diagram based on fracture of bottom steel layer

After the punching test, deformed EG–PA–EG sandwich composite specimens exhibited both steel fracture and delamination, as shown in Fig. 9. In this section, the formability of steel–polymer sandwich composites considering the fracture of the bottom steel is investigated. The experimental FLDs of the EG monolayer and EG–PA–EG sandwich composite are shown in Fig. 10(a) and Fig. 10(b), respectively. It is shown that the formability of the composite was improved compared to that of the monolayer skin, as observed in other studies of metal–polymer sandwich composites [38,39]. This can be explained by an initial defect parameter, which is one of the

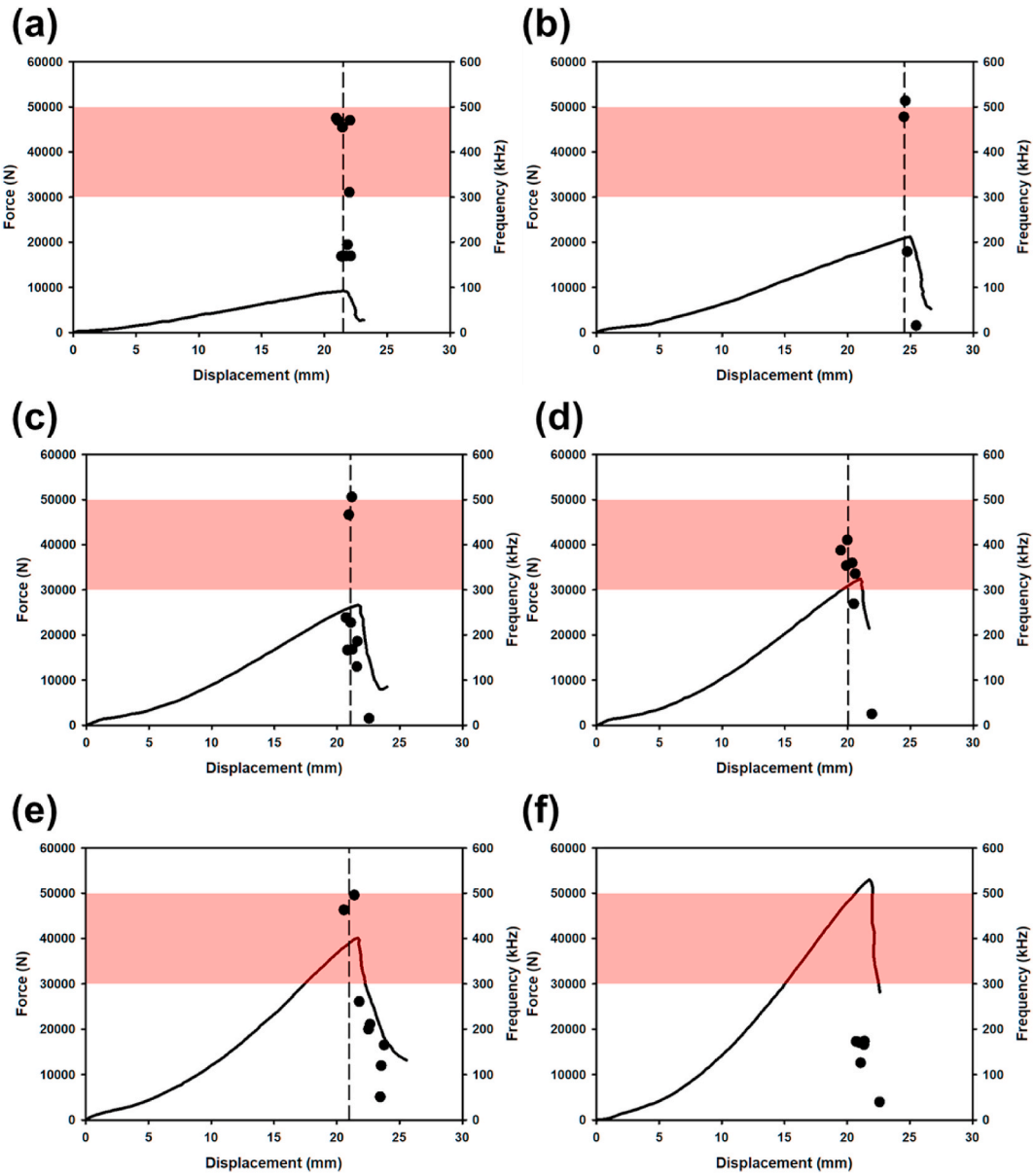

Fig. 11. Load as a function of displacement of the steel–polymer sandwich composite showing acoustic emission signals (dots), the moment of delamination (dashed line), and the delamination peak frequency band (red band). Samples (a) W10, (b) W20, (c) W30, (d) W40, (e) W50, and (f) W100. (color should be used). (For interpretation of the references to color in this figure legend, the reader is referred to the Web version of this article.)

major parameters affecting the formability of a sheet material [40]. As thickness of sandwich composites is larger than that of monolithic steel, initial defect becomes smaller and therefore, FLC of the sandwich composite shifted upward.

4.3. Forming limit diagram based on acoustic emission delamination signals

In this section, the formability of steel–polymer sandwich composites considering delamination is investigated. The load versus displacement plots obtained from the tests are overlaid with the peak frequency band plot of AE signals during the punching test. They are shown in Fig. 11(a)–(f). The red frequency band in the plot corresponds to the peak frequency band of delamination obtained from Section 4.1. The dashed line in the plot represents the average displacement of AE signals whose peak frequency falls within the range of the red band. Therefore, the dashed line indicates the moment of delamination during the punch test. In the W10 specimen, delamination occurred almost simultaneously with steel fracture, while in the W40 specimen, delamination occurred 4.5% earlier than steel fracture. No AE signals corresponding to delamination were observed in the W100 specimen. Based on these observations, it was

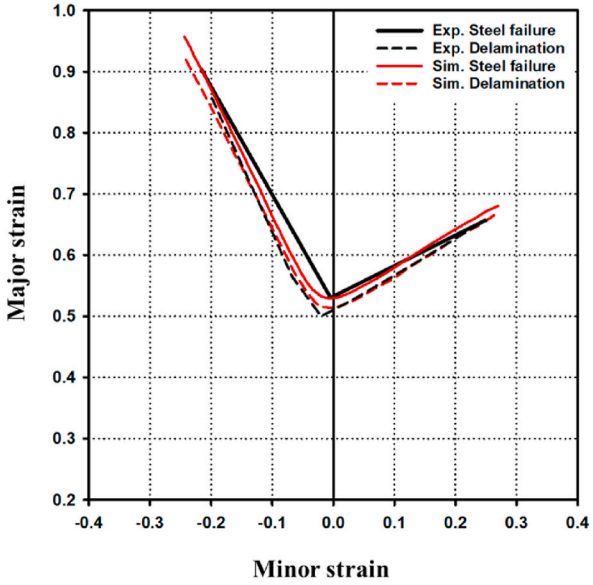

Fig. 12. Comparison between experimental and numerical FLD using the acoustic emission signal of delamination. (color should be used). (For interpretation of the references to color in this figure legend, the reader is referred to the Web version of this article.)

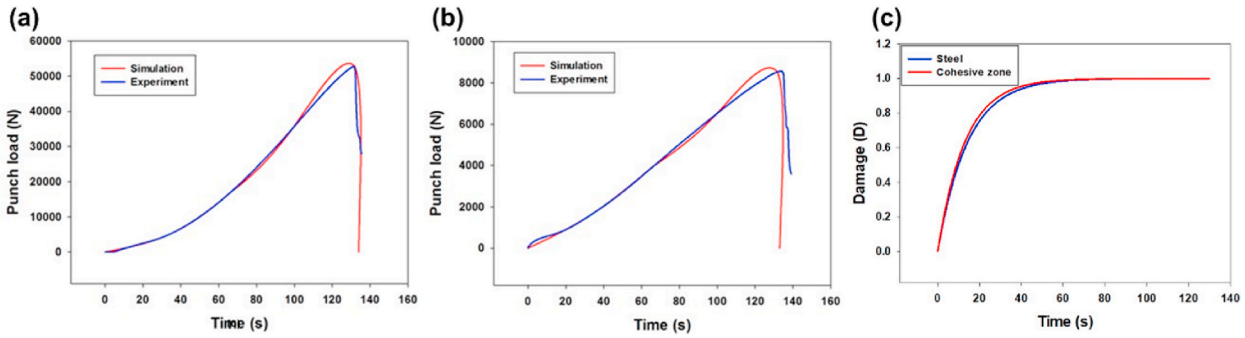

Fig. 13. Time as a function of punch load for (a) circular and (b) 10-mm wide sandwich composite specimens, and (c) changes in the damage factor of failed elements. (color should be used). (For interpretation of the references to color in this figure legend, the reader is referred to the Web version of this article.)

concluded that delamination rarely occurred under biaxial and uniaxial tension conditions. However, delamination was likely to occur rapidly when the minor strain of the sandwich composite approached zero.

To construct experimental FLD considering delamination, punch displacement corresponding to the dashed line in Fig. 11(a)–(f) was applied in the punch test. Then, major and minor strains of each specimen were measured. Finally, FLD based on delamination constructed as shown in Fig. 12. The FLD constructed by considering delamination (black dash line) was slightly lower than that based on skin steel fracture (black solid line). Therefore, it should be noted that if the AE features of failure mechanisms are identified through pre-tests, the Nakazima test with AE sensors can be used to characterize the formability of steel–polymer sandwich composites considering both steel fracture and delamination.

4.4. Numerical FLD

The validity of the analysis was confirmed by comparing the time-punch load curves obtained from experiment and simulation, which showed good agreement (Fig. 13(a) and (b)). The damage factors of steel and cohesive zones observed during the punch test simulation are shown in Fig. 13(c). When either damage factor reached 1, minor and major strains were extracted at that time step. Finally, a numerical FLD with interfacial properties was developed, as shown in Fig. 12. The FLD constructed by considering delamination was slightly lower than that based on specimen fracture, which was consistent with the experimental results. Although there was a slight difference between the uniaxial and biaxial tension conditions, the FLDs showed good agreement over a wide range of minor strain (from −0.1168 to 0.1360).

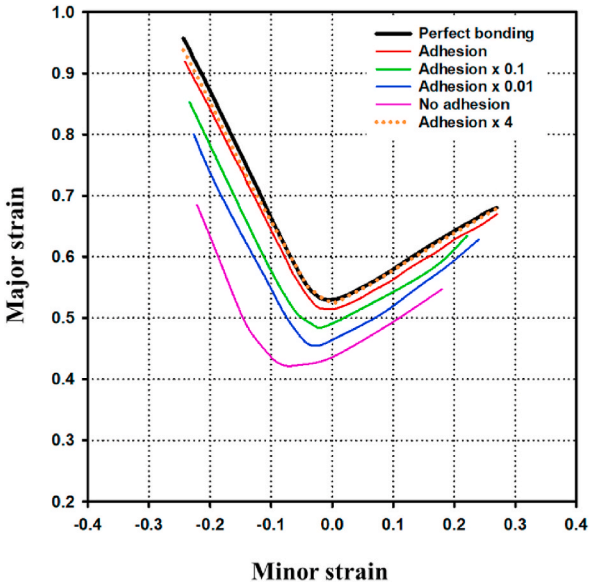

Fig. 14. Numerical FLD as a function of adhesion. (color should be used). (For interpretation of the references to color in this figure legend, the reader is referred to the Web version of this article.)

4.5. Effect of adhesion

Simulations were conducted to determine the effect of interfacial properties on the formability of the sandwich composite and predict the necessary interfacial properties for stable formability, by varying the mode I and II failure strengths while maintaining the same ratio. The results, shown in Fig. 14, indicate that the forming limit of the sandwich composite increased as the interfacial properties increased. The legend "Adhesion" represents the interfacial properties in the experiment, while the other legends indicate the multiples used to change the failure strength. In most cases, delamination at the interface occurred before specimen failure in the formability simulation, and weaker interfacial properties resulted in delamination at lower strain. Additionally, deterioration of formability due to a weak interface was greater when the minor strain approached zero. The optimal interfacial properties to ensure stable formability were indirectly identified through simulation, and the failure strengths at the interface during the formability test that prevent delamination should be at least four times higher than those of the interfacial properties confirmed experimentally.

5. Conclusion

In this study, we proposed a novel experimental approach for constructing forming limit diagram (FLD) to evaluate the formability of steel–polymer sandwich composites. Our approach relied on acoustic emission (AE) monitoring to detect delamination, which was identified by a peak frequency band in the range of 300–500 kHz. We also conducted numerical simulations using the cohesive zone model to investigate the effects of interfacial properties and damage on formability. Our results showed that stronger interfacial properties led to improved formability by reducing the risk of delamination. Overall, our approach provides a valuable tool for optimizing the design and processing of steel–polymer sandwich composites for various industrial applications.

Author contribution statement

Jewook Yang: Conceived and designed the experiments; Performed the experiments; Analyzed and interpreted the data; Contributed reagents, materials, analysis tools or data; Wrote the paper.

Sungjin Han: Analyzed and interpreted the data; Contributed reagents, materials, analysis tools or data; Wrote the paper.

Woong-Ryeol Yu: Conceived and designed the experiments; Contributed reagents, materials, analysis tools or data; Wrote the paper.

Data availability statement

The authors do not have permission to share data.

Declaration of competing interest

The authors declare that they have no known competing financial interests or personal relationships that could have appeared to

influence the work reported in this paper.

Acknowledgment

This work was supported by the National Research Foundation of Korea (NRF) grant funded by the Korea government (MSIT) (No. NRF-2020R1A5A6017701) and the Research center for Strategic materials by POSCO (No. 2018Z093).

References

[1] B. Engel, J. Buhl, Metal forming of vibration-damping composite sheets, Steel Res. Int. 82 (6) (2011) 626–631.
[2] S. Christke, et al., Multi-layer polymer metal laminates for the fire protection of lightweight structures, Mater. Des. 97 (2016) 349–356.
[3] G.W. Stachowiak, A.W. Batchelor, Engineering Tribology, Butterworth-heinemann, 2013.
[4] M. Fazlollahi, M.R. Morovvati, B. Mollaei Dariani, Theoretical, numerical and experimental investigation of hydro-mechanical deep drawing of steel/polymer/steel sandwich sheets, Proc. IME B J. Eng. Manufact. 233 (5) (2019) 1529–1546.
[5] S. Farahani, V.A. Yerra, S. Pilla, Analysis of a hybrid process for manufacturing sheet metal-polymer structures using a conceptual tool design and an analytical-numerical modelling, J. Mater. Process. Technol. 279 (2020), 116533.
[6] S. Mousa, G.-Y. Kim, A direct adhesion of metal-polymer-metal sandwich composites by warm roll bonding, J. Mater. Process. Technol. 239 (2017) 133–139.
[7] A. Qadeer, et al., Springback behavior of a metal/polymer laminate in incremental sheet forming: stress/strain relaxation perspective, J. Mater. Res. Technol. 23 (2023) 1725–1737.
[8] M. Harhash, H. Palkowski, Incremental sheet forming of steel/polymer/steel sandwich composites, J. Mater. Res. Technol. 13 (2021) 417–430.
[9] S. ASTM, Standard test method for determining forming limit curves, ASTM Int. West Conshohocken, PA 1 (1) (2008) 1.
[10] A. Forcellese, M. Simoncini, Mechanical properties and formability of metal–polymer–metal sandwich composites, Int. J. Adv. Des. Manuf. Technol. (2020) 1–17.
[11] M. Harhash, et al., Experimental characterization, analytical and numerical investigations of metal/polymer/metal sandwich composites–Part 2: free bending, Compos. Struct. 232 (2020), 111421.
[12] M. Parsa, M. Ettehad, Experimental and finite element study on the spring back of double curved aluminum/polypropylene/aluminum sandwich sheet, Mater. Des. 31 (9) (2010) 4174–4183.
[13] J. Liu, W. Liu, W. Xue, Forming limit diagram prediction of AA5052/polyethylene/AA5052 sandwich sheets, Mater. Des. 46 (2013) 112–120.
[14] O.A. Sokolova, A. Carrado, H. Palkowski, Metal–polymer–metal sandwiches with local metal reinforcements: a study on formability by deep drawing and bending, Compos. Struct. 94 (1) (2011) 1–7.
[15] M. Weiss, et al., The influence of temperature on the forming behavior of metal/polymer laminates in sheet metal forming, J. Eng. Mater. Techn. Trans. Asme 129 (4) (2007) 530–537.
[16] F. Kazemi, R. Hashemi, S.A. Niknam, Formability and fractography of AA5754/polyethylene/AA5754 sandwich composites, Mech. Base. Des. Struct. Mach. 50 (4) (2020) 1253–1267.
[17] Y.K. Son, D.C. Ko, B.M. Kim, Prediction of delamination and tearing during stamping of polymer-coated metal sheet, J. Mater. Process. Technol. 220 (2015) 146–156.
[18] K. Nakazima, T. Kikuma, K. Hasuka, Study on the formability of steel sheets, 1968, Yawata Tech. Rep. 264 (1968) 8517–8530.
[19] ISO, Metallic Materials–Sheet and Strip–Determination of Forming-Limit Curves–Part 2: Determination of Forming-Limit Curves in the Laboratory, ISO, 2008, pp. 1–27.
[20] M. Aghaie-Khafri, R. Mahmudi, Predicting of plastic instability and forming limit diagrams, Int. J. Mech. Sci. 46 (9) (2004) 1289–1306.
[21] E. ASTM, Standard test methods for tension testing of metallic materials, in: Annual Book of ASTM Standards, ASTM, 2001.
[22] ASTM, ASTM D638, Encyclopedic Dictionary of Polymers, 51, Springer, New York, 2011, p. 51.
[23] A.S.T.M. Strength, Properties of Adhesively Bonded Plastic Lap-Shear Sandwich Joints in Shear by Tension Loading, Annual Book of ASTM Standards, American Society for Testing Materials, Philadelphia, 1997.
[24] H. Hooputra, et al., A comprehensive failure model for crashworthiness simulation of aluminium extrusions, Int. J. Crashworthiness 9 (5) (2004) 449–463.
[25] F.X.C. Andrade, J.M.A.C. de Sa, F.M.A. Pires, Assessment and comparison of non-local integral models for ductile damage, Int. J. Damage Mech. 23 (2) (2014) 261–296.
[26] J. Jang, et al., Prediction of delamination of steel-polymer composites using cohesive zone model and peeling tests, Compos. Struct. 160 (2017) 118–127.
[27] R. Naik, S. Panda, V. Racherla, Failure analysis of metal-polymer-metal sandwich panels with wire mesh interlayers: finite element modeling and experimental validation, Compos. Struct. 280 (2022), 114813.
[28] G. Alfano, On the influence of the shape of the interface law on the application of cohesive-zone models, Compos. Sci. Technol. 66 (6) (2006) 723–730.
[29] L. Ye, Role of matrix resin in delamination onset and growth in composite laminates, Compos. Sci. Technol. 33 (4) (1988) 257–277.
[30] R. Long, Static strength of adhesively bonded ARALL-1 joints, J. Compos. Mater. 25 (4) (1991) 391–415.
[31] S. Han, et al., The effects of adhesion on the tensile strength of steel-polymer sandwich composites, Adv. Compos. Mater. 30 (5) (2020) 443–461.
[32] J.Z. Gronostajski, Z. Zimniak, Theoretical simulation of sheet behavior in forming processes, J. Mater. Process. Technol. 31 (1–2) (1992) 57–63.
[33] S. Panich, et al., Experimental and theoretical formability analysis using strain and stress based forming limit diagram for advanced high strength steels, Mater. Des. 51 (2013) 756–766.
[34] A. Kami, et al., Numerical determination of the forming limit curves of anisotropic sheet metals using GTN damage model, J. Mater. Process. Technol. 216 (2015) 472–483.
[35] R. Gutkin, et al., On acoustic emission for failure investigation in CFRP: pattern recognition and peak frequency analyses, Mech. Syst. Signal Process. 25 (4) (2011) 1393–1407.
[36] A. Monti, et al., Mechanical behaviour and damage mechanisms analysis of a flax-fibre reinforced composite by acoustic emission, Compos. Appl. Sci. Manuf. 90 (2016) 100–110.
[37] R. Mohammadi, et al., Correlation of acoustic emission with finite element predicted damages in open-hole tensile laminated composites, Compos. B Eng. 108 (2017) 427–435.
[38] J.G. Liu, W. Liu, W. Xue, Forming limit diagram prediction of AA5052/polyethylene/AA5052 sandwich sheets, Mater. Des. 46 (2013) 112–120.
[39] M.H. Parsa, M. Ettehad, P.H. Matin, Forming limit diagram determination of Al 3105 sheets and Al 3105/polypropylene/Al 3105 sandwich sheets using numerical calculations and experimental investigations, J. Eng. Mater. Techn. Trans. Asme 135 (3) (2013).
[40] K.J. Kim, et al., Formability of AA5182/polypropylene/AA5182 sandwich sheets, J. Mater. Process. Technol. 139 (1–3) (2003) 1–7.